Contrasting décollement and prism properties over the Sumatra 04-05 earthquake rupture boundary

Simon M. Dean[1], Lisa C. McNeill[1], Timothy J. Henstock[1], Jonathan M. Bull[1], Sean P.S. Gulick[2], James A. Austin, Jr.[2], Nathan L.B. Bangs[2], Yusuf S. Djajadihardja[3], Haryadi Permana[4]

Supporting Online Material

Materials and Methods

This supplementary document describes the seismic data acquisition parameters, processing steps, and velocity analysis method for the accompanying Dean et al. paper. This includes the method for calculating the reflection coefficient from amplitude values extracted from the data, and the associated energy transmission and absorption corrections made.

Seismic reflection data were acquired using a 2.4 km long, 192-channel digital streamer and a 12-G-gun tuned source with a total capacity of 5420 cu. in. (~89 l) at 2000 psi (~14 MPa). The shot interval of 18-20 s, depending on water depth, gave an average shot spacing of ~50 m and the data were processed with a CDP spacing of 6.25 m to give a fold of ~24.

We used ProMAX software to carry out Kirchhoff prestack depth migration of the data. The sediment velocity model for each line is derived using CRP velocity analysis and constructed using up to 10 layers chosen to follow key sediment reflectors (Fig. S1). The key reflectors were chosen based on high amplitude and strong lateral continuity, and tied in time at the intersections between profiles to produce consistent models. The velocity within each sediment layer has no vertical gradient; lateral velocity gradients are used where layer thickness changes significantly on the margin perpendicular profiles. A 1-dimensional water velocity model was derived from CTD measurements as a series of velocity gradient layers; the velocity structure below oceanic basement could not be constrained from the MCS data so we use an average oceanic crust velocity structure (*S1*) with a 2 km thick high-gradient layer (4.5-6.4 km/s) overlying a 5 km thick low-gradient layer (6.5-7.2 km/s), with an 8 km/s half-space representing the lithospheric mantle. To minimize step-related imaging artifacts the velocity model is smoothed using a triangular-weighted operator with a 200 m half-width below the seabed.

Uncertainty in the velocity model is difficult to quantify absolutely, but may be estimated. In general terms the thinner the model layer, the larger the uncertainty in velocity. Velocity uncertainty is also related to the depth to the reflector, making it more difficult to pick the correct velocity for a deep layer; an increased reflection depth reduces the maximum incidence angle and increases the seismic wavelength due to both attenuation and the general increase in seismic velocity with increasing depth. We estimate the velocity uncertainty for each layer in our model to be approximately ±0.2 km/s and do not attempt to resolve a layer less than 200 ms thick (~200-400 m depending on depth).

Final processed sections in the main paper (Figs. 2-4) are presented with a 2 km AGC window to enhance the visibility of structure beneath the prism. Sections with no post-migration amplitude adjustment show the relative reflection amplitude variations in the deep ocean sediment section and top of the oceanic basement (Figs. S2-S4). A trench wedge up to 2.5 km thick unconformably overlies a 1.2-1.5 km thickness of sediments on the incoming Indian Plate (Figs. 2-4). Sediment velocity at the trench northwest of Simeulue (Fig. S1) increases almost linearly from ~1.85 km/s at the seabed to 3-3.5 km/s at the base of the trench wedge, with a rapid increase to ~4 km/s in the deep ocean sediment section. Seismic velocity southeast of the 2004-2005 rupture boundary is similar within the trench wedge, but the sediment velocity does not measurably increase into the deep ocean sediment section.

To eliminate the possibility of processing-related artefacts, we determined reflection amplitudes and waveforms from unstacked data with a minimum phase bandpass filter with corner frequencies of 3-5-60-120 Hz. We use a correction for 1/r spherical divergence. We extracted maximum amplitudes from within a narrow time window centered on picked reflection times (Fig. S5); a normal moveout (NMO) correction is applied to flatten reflectors in the offset domain. The source output is calibrated using the ratio between the amplitudes of the seabed reflection and the first seabed multiple (*S2*). For deeper reflectors a correction is applied for the two-way transmission of energy at the seabed and for absorption for a reflection with 25 Hz peak amplitude, obtained by spectral analysis, and assuming an average Q of 200; we assume the energy loss from transmission through layers within the sediments is negligible. Our chosen Q value is at the upper limit for sedimentary rock (*S3*), thus our calculated absorption is a minimum and our reflection coefficient represents a lower bound estimate (Table S1).

Reflected waveforms

The reflected waveforms for the HA-NP reflector northwest (Fig. 2), and the reflector southeast (Fig. S6) of the 04-05 rupture boundary, were derived from the unmigrated (time) data using an NMO correction for the migration velocity model and CDP stack.

Earthquake catalogue data

In the main paper we show aftershocks from the ISC catalogue. These are located using teleseismic data and hence absolute epicentres are potentially mislocated, however the relative pattern of locations is likely to be correct over the small study area. Three studies using local networks (*S4*, *S5*, *S6*) show robustly that the aftershocks within the region where the pre-decollement reflector is present extend to the trench, whereas aftershocks immediately to the southeast do not. In the main paper we nevertheless retain the ISC locations as they allow us to distinguish the two aftershock series, whereas the local deployment covering the transition (*S4*) occurred after the 2005 earthquake, so can not distinguish the two series.

Figures

Fig. S1

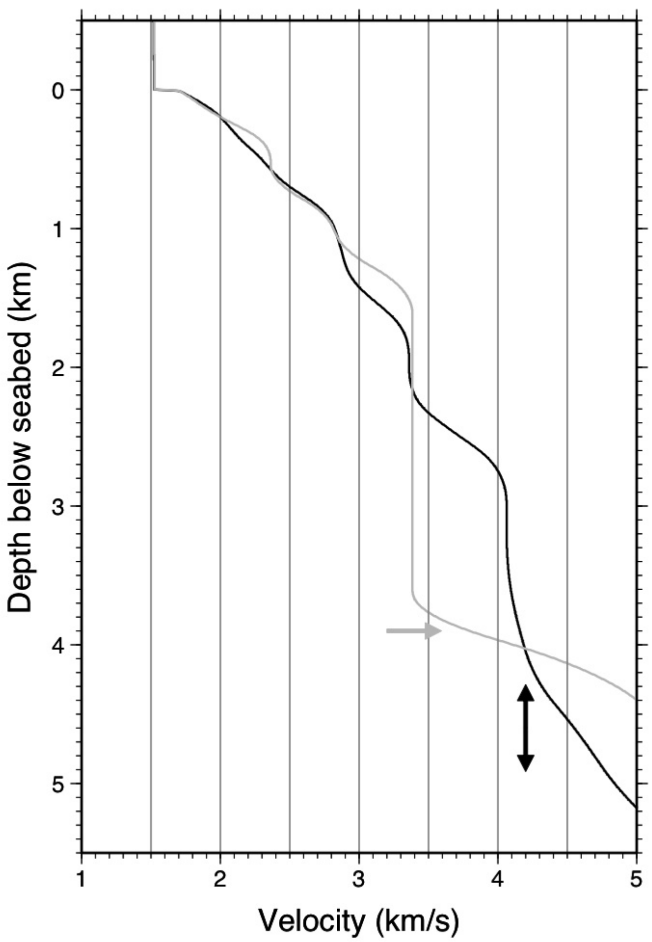

Fig. S1: Velocity structure for the incoming deep ocean sediment section close to the deformation front and northwest of Simeulue (black line; mean from five profiles), and south of ~1°30'N (gray line; profile C-C'); arrows identify top of oceanic basement. Upper 2 km of sediment section has equivalent velocities in both regions, whereas the section from 2.5-4 km depth beneath the seabed has higher velocity in the area where the pre-decollement reflection is found.

Fig. S2

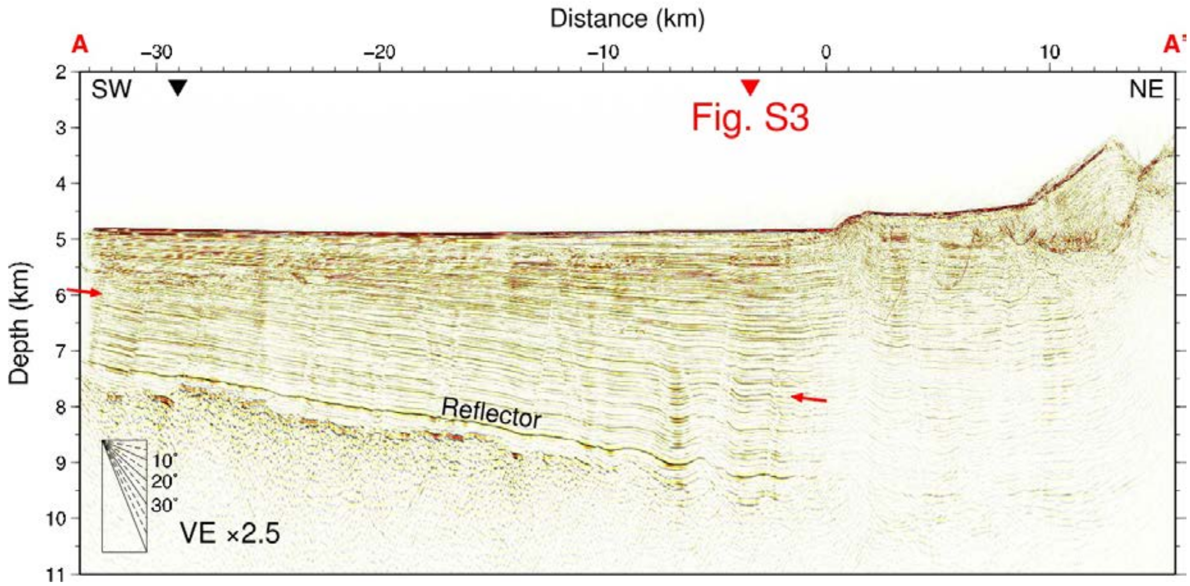

Fig. S2: Depth migrated seismic profile A-A’, as Fig. 2 with no AGC applied.

Fig. S3

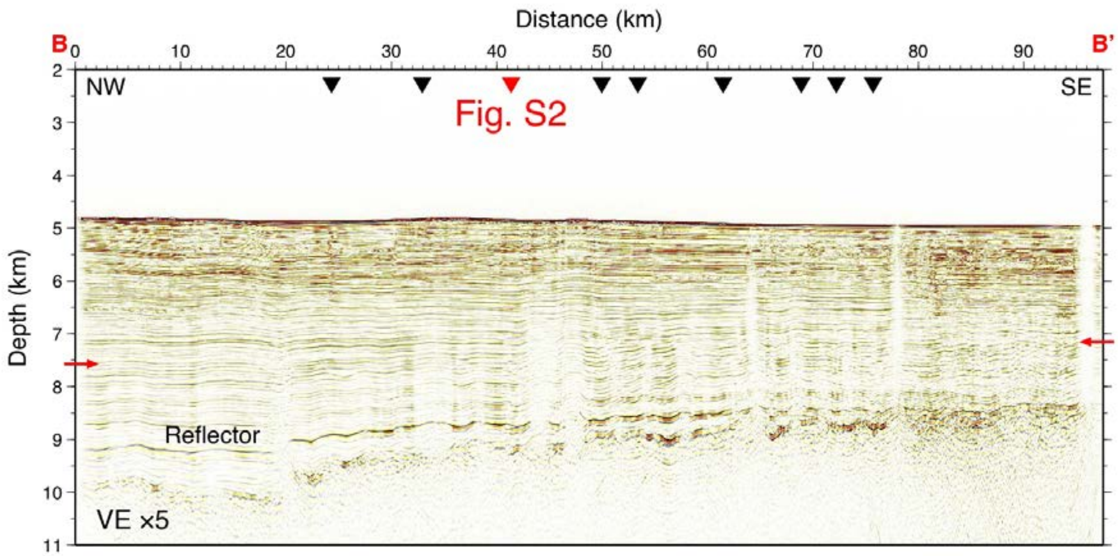

Fig. S3: Depth migrated seismic profile B-B', as Fig. 3 with no AGC applied.

Fig. S4

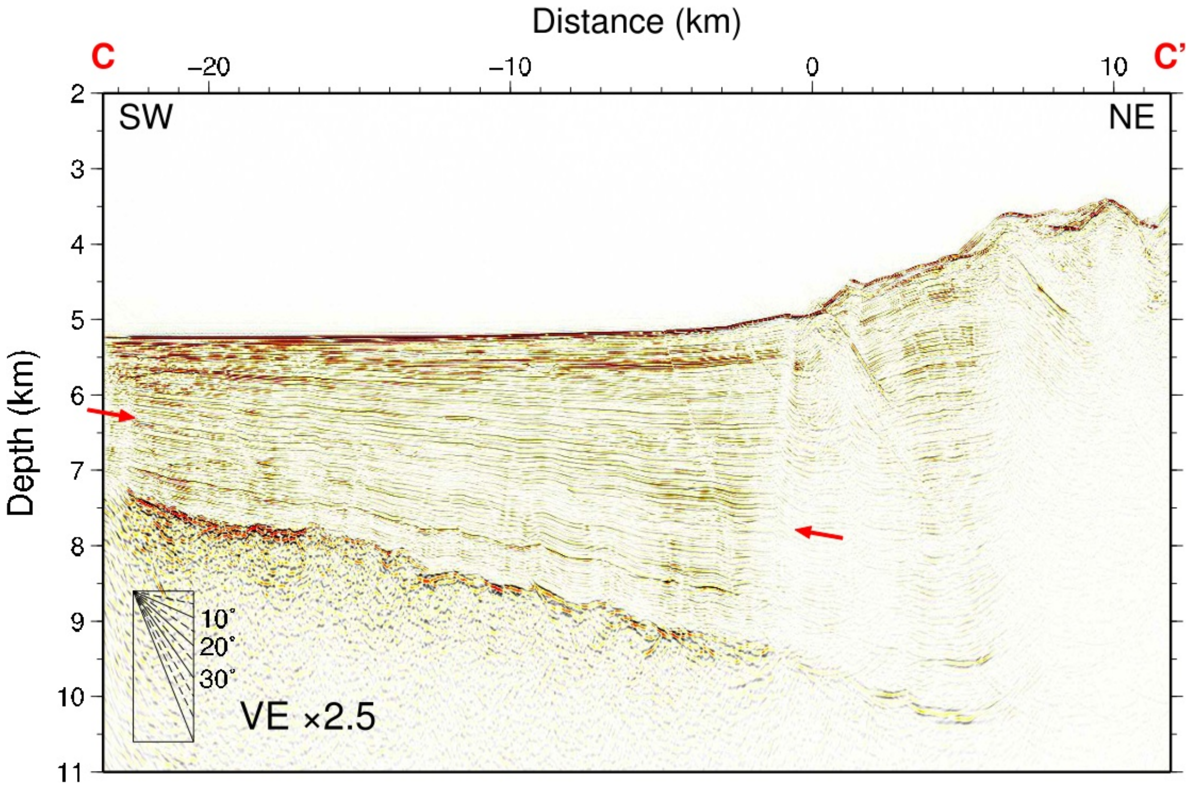

Fig. S4: Depth migrated seismic profile C-C', as Fig. 4 with no AGC applied.

Fig. S5

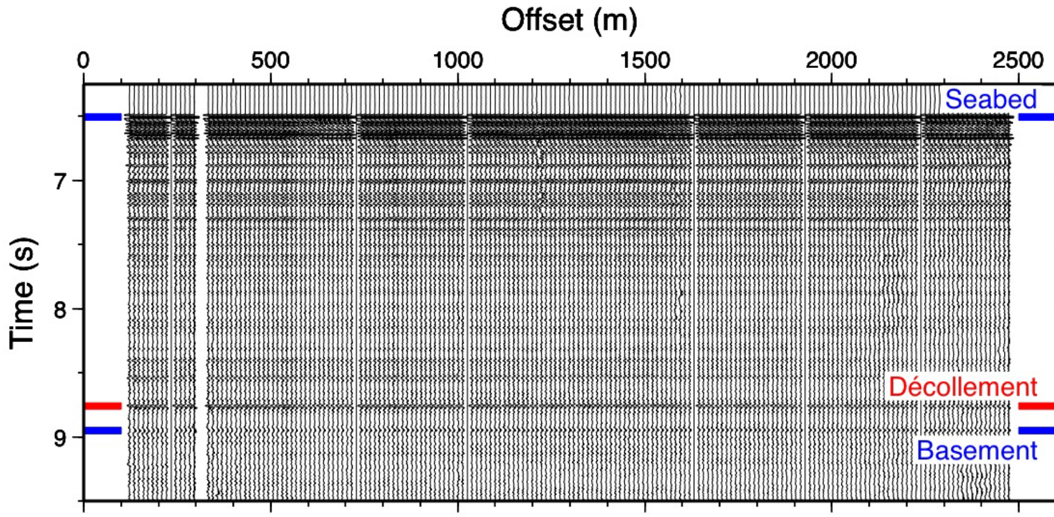

Fig. S5: Unstacked MCS data from profile A-A' (Fig. 2) with bandpass filter and spherical divergence correction as described in the text. Significant reflectors are identified; line thickness represents the time window within which amplitudes are extracted for analysis (±25 ms).

Fig. S6

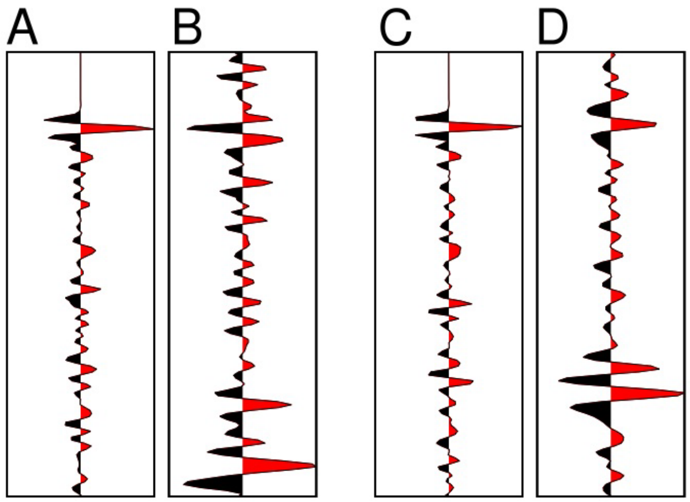

Fig. S6: Reflected waveforms from seismic profile C-C’ (Fig. 4) at the seabed (A and C) and the reflector, superficially similar to the pre-decollement reflector identified northwest of the 04-05 rupture boundary, but with significantly lower amplitude (weaker than top oceanic basement) and variable polarity (B and D), traces aligned with the seabed.

Tables

Q	Reflection coefficient
75	-0.443
100	-0.248
150	-0.139
200	-0.104
250	-0.087

Table S1: Reflection coefficient of the décollement reflector estimated for a seismic signal of 25 Hz, assuming overlying sediment with an average Q of between 75 and 250.

References

S1. R. S. White, D. P. McKenzie, R. K. O'Nions, *J. Geophys. Res.* **97**, 19683-19715 (1992).

S2. M. Warner, *Tectonophysics* **173**, 15-23 (1990).

S3. R. E. Sheriff, L. P. Geldart, *Exploration Seismology* (Cambridge Univ. Press, Cambridge, ed. 2, 1995).

S4. F. Tilmann *et al.*, *Geophys. J. Int.*, in press.

S5. J.-Y. Lin, X. Le Pichon, C. Rangin, J.-C. Sibuet, T. Maury, *Geochem. Geophys. Geosyst.* **10**, Q05006, doi:10.1029/2009GC002454 (2009).

S6. E. Araki *et al.*, *Earth Planets Space* **58**, 113-119 (2006).